COMPUTER METHODS IN APPLIED MECHANICS AND ENGINEERING 16 (1978) 101–115
NORTH-HOLLAND PUBLISHING COMAPNY

THREE-DIMENSIONAL ANALYSIS OF NONLINEAR MAGNETOSTATIC FIELDS IN A SATURABLE REACTOR

Yoshifuru SAITO

Electrical Department, College of Engineering, Hosei University, Kajinocho Koganei 184, Tokyo, Japan

Manuscript received 28 December 1977

The nonlinear magnetostatic fields in a saturable reactor are calculated by the method of magnetic circuits.

Notation

$\boldsymbol{A}$	vector potential
$\mathrm{d}a$	infinitesimally small area
$\mathrm{d}\boldsymbol{l}$	infinitesimally small distance
g	mesh spacing in direction of y-axis
$\boldsymbol{H}$	magnetic field intensity [AT/m]
h	mesh spacing in direction of x-axis
I	current [A]
$\boldsymbol{J}$	current density [$\mathrm{A/m^2}$]
$\boldsymbol{n}$	unit normal vector
p	mesh spacing in direction of z-axis
$\boldsymbol{R}_{i\pm(1/2)}, \boldsymbol{R}_{j\pm(1/2)}$	magnetic resistances around the mesh point (i, j) in direction of x-axis and of y-axis, respectively
$\boldsymbol{R}_i^{(1)}, \boldsymbol{R}_j^{(1)}$	magnetic resistances as functions of permeability $\mu_{i,j}^{(1)}$ in direction of x-axis and of y-axis, respectively
$\boldsymbol{R}_{i+1}^{(3)}$	magnetic resistance as function of permeability $\mu_{i+1,j}^{(3)}$ in direction of x-axis
$\boldsymbol{R}_{j-1}^{(2)}$	magnetic resistance as function of permeability $\mu_{i,j-1}^{(2)}$ in direction of y-axis
$S_{i,j}$	surface area bounded by contour $\overline{abcd}$
U	scalar potential [AT]
ε	mean percentage error in entire solution
μ	$= f(\mathrm{grad}\ U)$, permeability as function of rate of change of potential U
ϕ	magnetic flux [Wb]
ω	relaxation parameter
$\Delta\omega$	rate of change of relaxation parameter

Superscripts 1, 2, 3, 4 refer respectively to the permeabilities $\mu^{(1)}$, $\mu^{(2)}$, $\mu^{(3)}$, $\mu^{(4)}$ in each of the regions; K indicates the Kth complete iteration. Subscripts $i, i \pm 1, i \pm (1/2), j, j \pm 1, j \pm (1/2)$ refer respectively to the positions $x_i, x_i \pm h, x_i \pm (h/2), y_j, y_j \pm g, y_j \pm (g/2)$; $\overline{abcd}, \overline{eb}, \overline{bf}$ denote the con-

tour lines. Moreover, M and m denote respectively the total number of loop magnetic fluxes and the number of small magnetic resistances with the shape of a rectangular prism.

1. Introduction

The calculation of magnetic fields is the basis of the design of all electromagnetic devices such as transformers, reactors and electrical rotating machines. With the development of modern electromagnetic devices the nonlinear magnetization characteristic of iron must be taken into account in the design. Because of the nonlinear magnetization characteristic of the iron parts in electromagnetic devices it is difficult to calculate the magnetic fields analytically.

However, when modern digital computers came into wide use, numerical methods became available to calculate the magnetic fields of electromagnetic devices, taking into account the nonlinear magnetization characteristic of iron.

The numerical methods are fundamentally divided into two clases: (1) the finite difference method, which was extensively applied to electrical rotating machines by Erdélyi and his associates [1–6], and (2) the finite element method, which was applied to transformers as well as electrical rotating machines by Silvester and others [7–12].

The author has reported the method of magnetic circuits for the calculation of magnetostatic fields in current-free region (scalar potential problem) [13]. The purpose of the present paper is to develop the method of magnetic circuits as a means of calculating three-dimensional magnetostatic fields in a saturable reactor. Since the method of magnetic circuits was developed to solve the scalar potential problem, a serious difficulty arises when the method is applied to the vector potential problem. However, this difficulty is avoided by replacing the uniformly distributed current by concentrating on the infinitesimally small conductor. Appendix A shows that the magnetic circuit equation in this paper is one of the finite difference equations.

A system of magnetic circuit equations is efficiently solved by the iteration method, using a relaxation parameter which is determined in appendix B.

2. Fundamental equation based on magnetic circuits

Consider the region bounded by the contour $\overline{abcd}$ in fig. 1a. It is possible to write the fundamental relation between the magnetic field intensity $\boldsymbol{H}$ and current density $\boldsymbol{J}_{i,j}$ as

$$\int_{abcd} \boldsymbol{H}^{\mathrm{t}} \mathrm{d}\boldsymbol{l} = \int_{S_{i,j}} \boldsymbol{J}_{i,j}^{\mathrm{t}} \boldsymbol{n} \, \mathrm{d}a \,, \tag{1}$$

where $\mathrm{d}\boldsymbol{l}$ denotes the infinitesimally small distance along the contour $\overline{abcd}$, $\mathrm{d}a$ is the infinitesimally small area, $S_{i,j}$ is the surface area bounded by the contour $\overline{abcd}$, and $\boldsymbol{n}$ is the unit normal vector on the infinitesimally small area $\mathrm{d}a$. Moreover, the subscripts i, j refer to the mesh point in fig. 1a. The right-hand term in eq. (1) is equivalent to the current $I_{i,j}$ through the surface $S_{i,j}$, viz.

$$\int_{S_{i,j}} \boldsymbol{J}_{i,j}^{\mathrm{t}} \boldsymbol{n} \, \mathrm{d}a = I_{i,j} \,. \tag{2}$$

In order to apply the method of magnetic circuits to the region bounded by the contour $\overline{abcd}$ in fig. 1a, it is assumed that the current $I_{i,j}$ in eq. (2) is not uniformly distributed on the surface

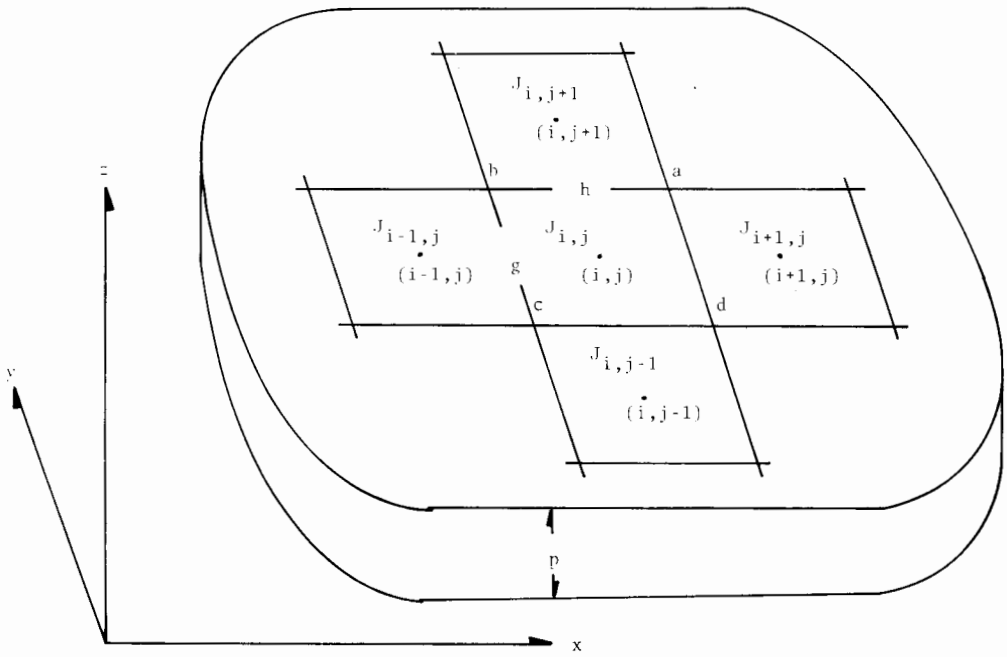

Fig. 1a. General mesh point.

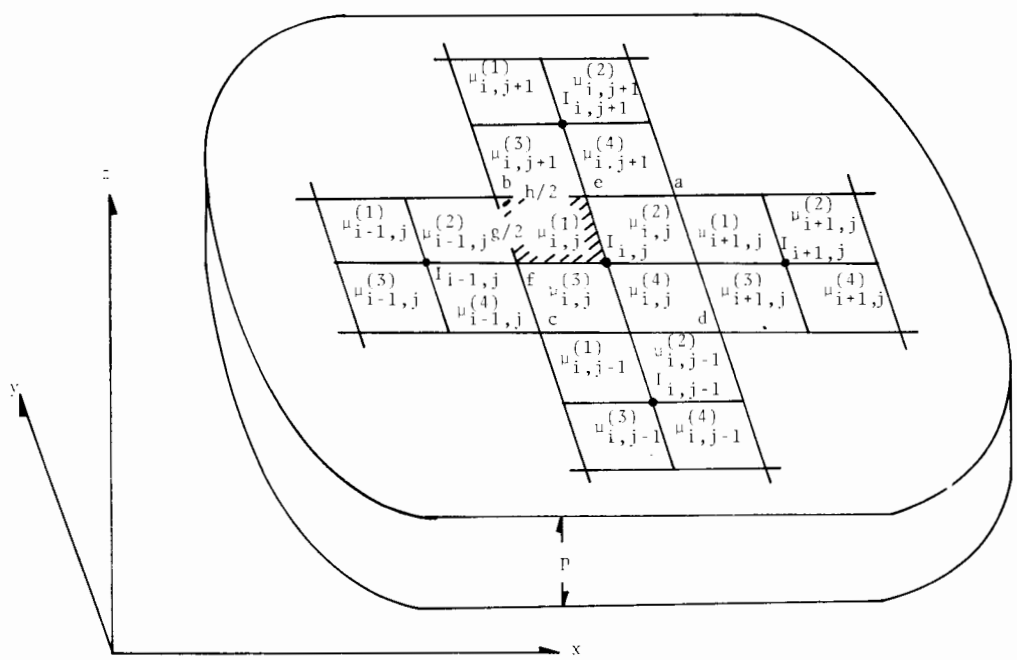

Fig. 1b. Modified representation of fig. 1a.

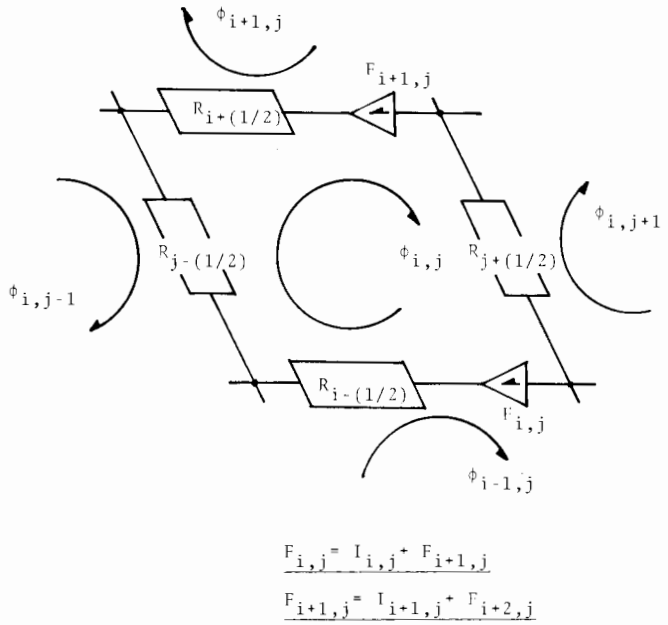

Fig. 1c. Magnetic circuit representation ($F_{i,j}$, $F_{i+1,j}$ denote the magnetomotive forces).

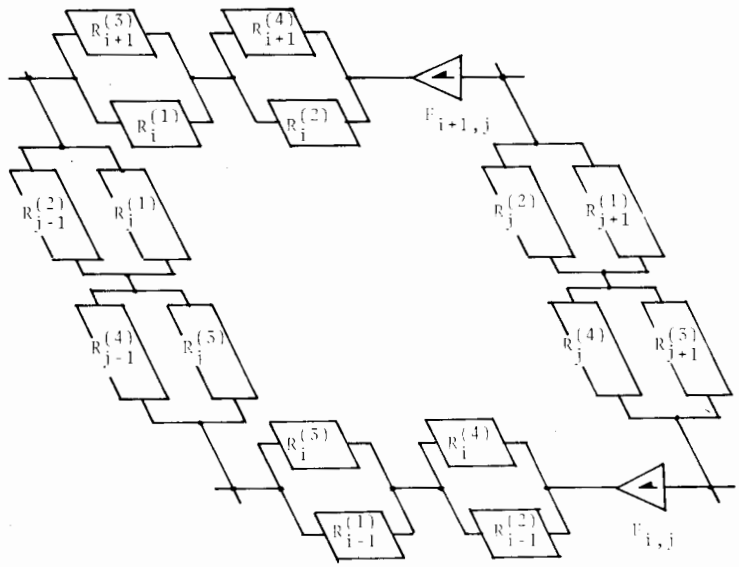

Fig. 1d. Details of magnetic circuit ($F_{i,j}$, $F_{i+1,j}$ denote the magnetomotive forces).

$S_{i,j}$ but concentrated on the conductor with infinitesimally small cross-sectional area located at the mesh point (i, j) in fig. 1a. Similarly, it is assumed that the currents in the other regions in fig. 1a are concentrated on the conductors with infinitesimally small cross-sectional area located at each of their mesh points.

Due to the nonlinear magnetization characteristic of iron, the permeability μ at each position

takes different value with respect to the position. Therefore, it is assumed that the region which encloses these mesh points in fig. 1a is divided into four subdivisions in each of which the permeability μ may have a distinct value.

With these assumptions the magnetic fields in fig. 1a may be calculated for a modified form in the region as shown in fig. 1b. This means that the calculation can be carried out by the method of magnetic circuits, taking into account the nonlinear magnetization characteristic of iron.

In the region bounded by contour $\overline{abcd}$ in fig. 1b the relation between the magnetic field intensity $\boldsymbol{H}$ and scalar potential $U_{\overline{abcd}}$ is given by

$$\int_{\overline{abcd}} \boldsymbol{H}^{\mathrm{t}} \mathrm{d}\boldsymbol{l} = U_{\overline{abcd}} \,. \tag{3}$$

In fig. 1b let $\phi_{i,j}$, $\phi_{i+1,j}$, $\phi_{i-1,j}$, $\phi_{i,j+1}$, $\phi_{i,j-1}$ denote the loop magnetic fluxes enclosing each of their mesh points, and let $\boldsymbol{R}_{i+(1/2)}$, $\boldsymbol{R}_{i-(1/2)}$, $\boldsymbol{R}_{j+(1/2)}$, $\boldsymbol{R}_{j-(1/2)}$ denote the magnetic resistances around the mesh point (i, j); then the magnetic circuit equation related to the scalar potential $U_{\overline{abcd}}$ in eq. (3) is formally written as

$$\boldsymbol{R}_{i+(1/2)}(\phi_{i,j} - \phi_{i+1,j}) + \boldsymbol{R}_{j-(1/2)}(\phi_{i,j} - \phi_{i,j-1}) + \boldsymbol{R}_{i-(1/2)}(\phi_{i,j} - \phi_{i-1,j}) + \boldsymbol{R}_{j+(1/2)}(\phi_{i,j} - \phi_{i,j+1}) = U_{\overline{abcd}} \,, \tag{4}$$

where the loop magnetic fluxes $\phi_{i,j}$, $\phi_{i+1,j}$, $\phi_{i-1,j}$, $\phi_{i,j+1}$, $\phi_{i,j-1}$ are taken positive in the clockwise direction, as shown in fig. 1c. By means of eqs. (1)–(4) it is possible to represent the magnetic circuit equation as

$$\boldsymbol{R}_{i+(1/2)}(\phi_{i,j} - \phi_{i+1,j}) + \boldsymbol{R}_{j-(1/2)}(\phi_{i,j} - \phi_{i,j-1}) + \boldsymbol{R}_{i-(1/2)}(\phi_{i,j} - \phi_{i-1,j}) + \boldsymbol{R}_{j+(1/2)}(\phi_{i,j} - \phi_{i,j+1}) = I_{i,j} . \tag{5}$$

Appendix A shows that eq. (5) is one of the finite difference equations. As shown in fig. 1d, the magnetic resistances $\boldsymbol{R}_{i+(1/2)}$, $\boldsymbol{R}_{i-(1/2)}$, $\boldsymbol{R}_{j+(1/2)}$, $\boldsymbol{R}_{j-(1/2)}$ are respectively decomposed into four magnetic resistances by the difference of permeabilities (see fig. 1b).

The magnetic resistance is generally defined by

$$\text{magnetic resistance} = \frac{\text{length of the flux path}}{\left[\begin{matrix}\text{permeability} \\ \text{of the material}\end{matrix}\right]\left[\begin{matrix}\text{cross-sectional area} \\ \text{normal to the flux path}\end{matrix}\right]} \,. \tag{6}$$

Some examples of magnetic resistance with typical shapes are listed in table 1. By the definition of eq. (6) it is possible to calculate the magnetic resistances $\boldsymbol{R}_{xA}$, $\boldsymbol{R}_{zB}$ in table 1. However, eq. (6) is not directly applicable to calculate the magnetic resistances $\boldsymbol{R}_{xB}$, $\boldsymbol{R}_{yB}$, $\boldsymbol{R}_{xC}$, $\boldsymbol{R}_{yC}$ because the length of the flux path of cross-sectional area normal to the flux path differs according to the positions. Therefore, in case of (B) in table 1, it is assumed that the magnetic resistance $\boldsymbol{R}_{y,B}$ is composed of a large number of series-connected small magnetic resistances that are similar in shape to the magnetic resistance $\boldsymbol{R}_{xA}$. Let m denote the number of series-connected small magnetic resistances; then the magnetic resistance $\boldsymbol{R}_{yB}$ in table 1 is calculated by

Table 1. Examples of magnetic resistance

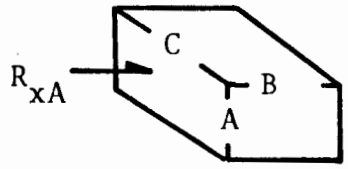

$$R_{xA} = \frac{B}{\mu AC}$$

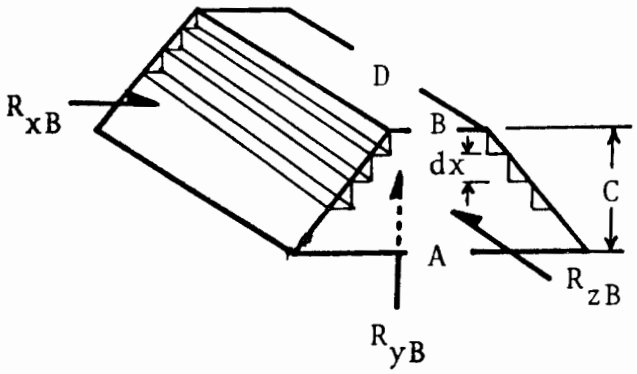

$$R_{xB} = \frac{A-B}{\mu CD \log(A/B)}$$

$$R_{yB} = \frac{C \log(A/B)}{\mu(A-B)D}$$

$$R_{zB} = \frac{2D}{\mu(A+B)C}$$

$$dx \cong \Delta x = C/m$$

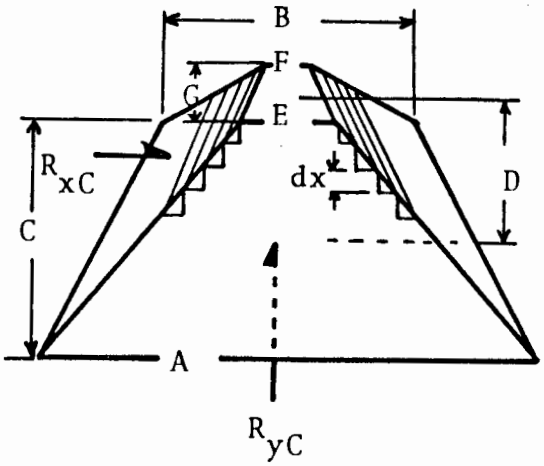

$$R_{xC} = \frac{1}{\mu \int_0^D \frac{G+\{(C-G)/D\}x}{E-F+\{(A-B+F-E)/D\}x} \log\left[\frac{E+\frac{A-E}{D}x}{F+\frac{B-F}{D}x}\right] dx}$$

$$R_{yC} = \frac{2}{\mu} \int_0^D \frac{dx}{\left[G+\frac{C-G}{D}x\right]\left[E+F+\frac{(A+B)-(E+F)}{D}x\right]}$$

$$dx \cong \Delta x = D/m$$

$$R_{yB} = \frac{C/m}{\mu DB} + \frac{C/m}{\mu D[B+(A-B)/m]} + \frac{C/m}{\mu D[B+(A-B)2/m]} + \frac{C/m}{\mu D[B+(A-B)(m-1)/m]}$$

$$= \frac{1}{\mu D} \sum_{k=0}^{m-1} \frac{C/m}{[B+\{(A-B)/C\}(kC/m)]}, \tag{7}$$

where the constants A, B, C, D are shown in table 1. In the limit $m \to \infty$ eq. (7) reduces to

$$R_{yB} = \frac{1}{\mu D} \int_0^C \frac{dx}{B+\{(A-B)/C\}x} = \frac{C}{\mu D(A-B)} \log(A/B), \tag{8}$$

obtained by defining

$$\Delta x = C/m \tag{9}$$

and

$$x_k = k\Delta x\,, \qquad k = 0,\ 1,\ \ldots\ m\,, \tag{10}$$

and placing the points x_k in the internal $[0, C]$ before applying the definition of the Riemann integral.

Similarly, it is assumed that the magnetic resistance $\boldsymbol{R}_{xB}$ in table 1 is composed of large number of parallel-connected small magnetic resistances that are similar in shape to the magnetic resistance $\boldsymbol{R}_{xA}$. Then the magnetic resistance $\boldsymbol{R}_{xB}$ in table 1 is given by

$$\boldsymbol{R}_{xB} = \lim_{m\to\infty}\left[\frac{1}{\mu D\sum_{k=0}^{m-1}\dfrac{C/m}{[B+\{(A-B)/C\}\,(kC/m)]}}\right] = \frac{1}{\mu D\displaystyle\int_0^C \frac{\mathrm{d}x}{B+\{(A-B)/C\}x}} = \frac{A-B}{\mu CD\log(A/B)}\,. \tag{11}$$

The formulas in table 1 for the magnetic resistances $\boldsymbol{R}_{xC}, \boldsymbol{R}_{yC}$ are obtained by making assumptions similar to those used in calculating of $\boldsymbol{R}_{xB}, \boldsymbol{R}_{yB}$.

In the region containing air the permeability μ is constant. However, in the region containing iron μ depends on the rate of change of scalar potential U at each position, that is

$$\mu = f(\mathrm{grad}\ U)\,, \tag{12}$$

where $f(\mathrm{grad}\ U)$ denotes a function of grad U. By considering figs. 1b–1d the rates of change of potentials $U_{\overline{eb}}$ and $U_{\overline{bf}}$ are approximately given by

$$\frac{\partial U_{\overline{eb}}}{\partial x} = \frac{U_{\overline{eb}}}{(h/2)} = \left(\frac{2}{h}\right)\left(\frac{\boldsymbol{R}_i^{(1)}\boldsymbol{R}_{i+1}^{(3)}}{\boldsymbol{R}_i^{(1)}+\boldsymbol{R}_{i+1}^{(3)}}\right)(\phi_{i,j}-\phi_{i+1,j})\,, \tag{13}$$

$$\frac{\partial U_{bf}}{\partial y} = \frac{U_{bf}}{(g/2)} = \left(\frac{2}{g}\right)\left(\frac{\boldsymbol{R}_j^{(1)}\boldsymbol{R}_{j-1}^{(2)}}{\boldsymbol{R}_j^{(1)}+\boldsymbol{R}_{j-1}^{(2)}}\right)(\phi_{i,j}-\phi_{i,j-1})\,, \tag{14}$$

where h and g denote respectively the mesh spacings in the directions of the x-axis and y-axis in fig. 1b; the magnetic resistances $\boldsymbol{R}_i^{(1)}, \boldsymbol{R}_j^{(1)}, \boldsymbol{R}_{i+1}^{(3)}, \boldsymbol{R}_{j-1}^{(2)}$ and the loop magnetic fluxes $\phi_{i,j}$, $\phi_{i+1,j}$, $\phi_{i,j-1}$ are shown in figs. 1c, 1d. By substituting eqs. (13), (14) into eq. (12) it is possible to obtain the permeability $\mu_{i,j}^{(1)}$ of the shadowed portion in fig. 1b. The permeabilities of the other portions in fig. 1b can be obtained in a similar manner.

3. Nonlinear magnetostatic fields in a saturable reactor

Since the magnetic flux which passes through the path parallel to the current-carrying coils can be neglected, it is preferable to consider the solid element as shown in fig. 2. The permeability of the solid element is determined from the mean rate of change of potential in the tangential direction as well as the rate of change of potential in the radial direction. Also the central portion of the solid element shown in fig. 2 is one of the elements, and the permeability of this element becomes a function of the mean rate of change of potential in the tangential direction because the magnetic resistance in radial the direction reaches an infinitely large value. The magnetic resistances in fig. 2 correspond to those in table 1.

The saturable reactor shown in fig. 3 subdivided in much the same way as the solid element shown in fig. 2 taking into account the region containing air; thus for a saturable reactor the calculation of three-dimensional magnetic fields can be carried out in a two-dimensional coordinate system (which consists of the tangential and radial directions) without committing any appreciable error. The nonlinear magnetization characteristic of iron is established by careful measurement on the saturable reactor. In carrying out the magnetic field calculation of the saturable reactor the nonlinear magnetization characteristic of the iron part of the reactor is introduced by linear interpolation [14].

Let there by M loop magnetic fluxes on the magnetic equivalent circuit of the saturable reactor

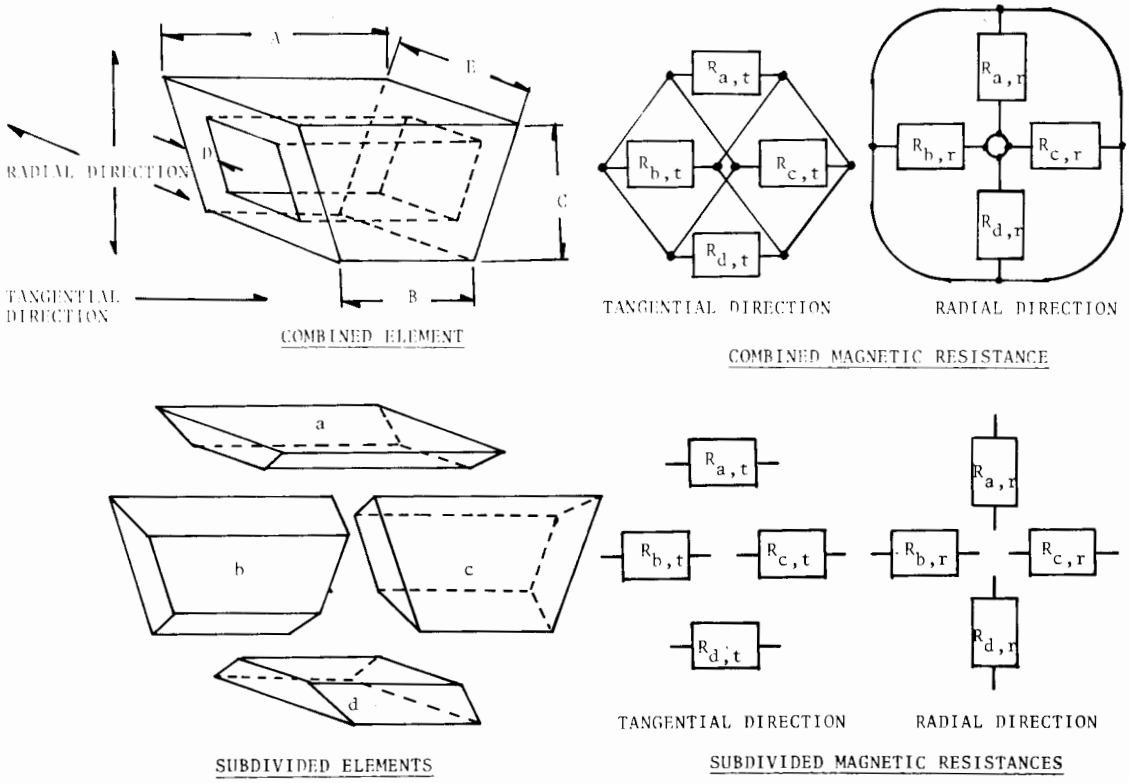

Fig. 2. Solid element and its magnetic resistances.

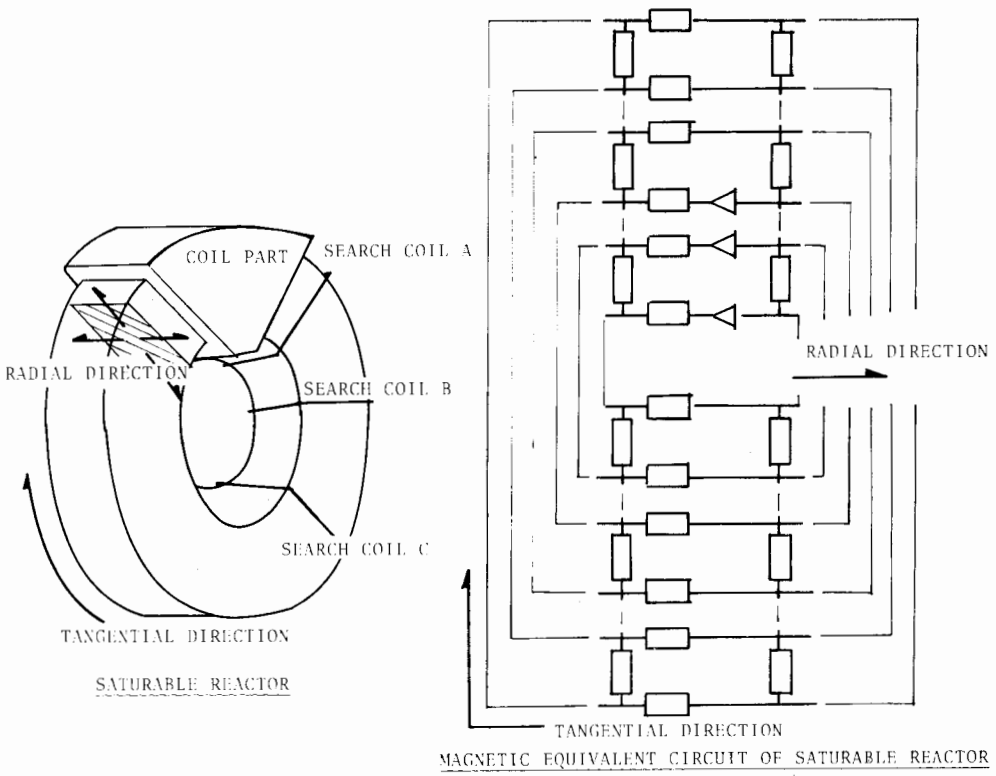

Fig. 3. Schematic diagram of saturable reactor and its magnetic equivalent circuit.

shown in fig. 3; the calculation of these fluxes reduces to the solution of a system of M simultaneous nonlinear algebraic equations since the magnetic circuit equation that takes into account the nonlinear magnetization characteristic of iron is one of the nonlinear algebraic equations. This system of M simultaneous nonlinear algebraic equations is solved by iteration using a relaxation parameter [13]. Fig. 4 shows the flow chart of this iteration method. The relaxation parameter is sequentially determined in every complete iteration by the method described in appendix B. Various constants used in the calculation of the saturable reactor are listed in table 2. Fig. 5a shows an example of the convergence process of the numerical solution. Some examples of numerical solutions are shown in fig. 5b together with experimental results which were obtained by the search coils shown in fig. 3 and were in fair agreement with the calculated values. Fig. 5c shows one of the magnetic flux distributions on the magnetic equivalent circuit in fig. 3.

4. Conclusion

In this paper it has been shown that the method of magnetic circuits is applicable to the scalar potential problem as well as the vector potential problem. Consequently, three-dimensional magnetostatic fields of a saturable reactor has been preditermined by the method of magnetic circuits. In particular, the method of magnetic circuits is effectively applicable to the three-dimensional

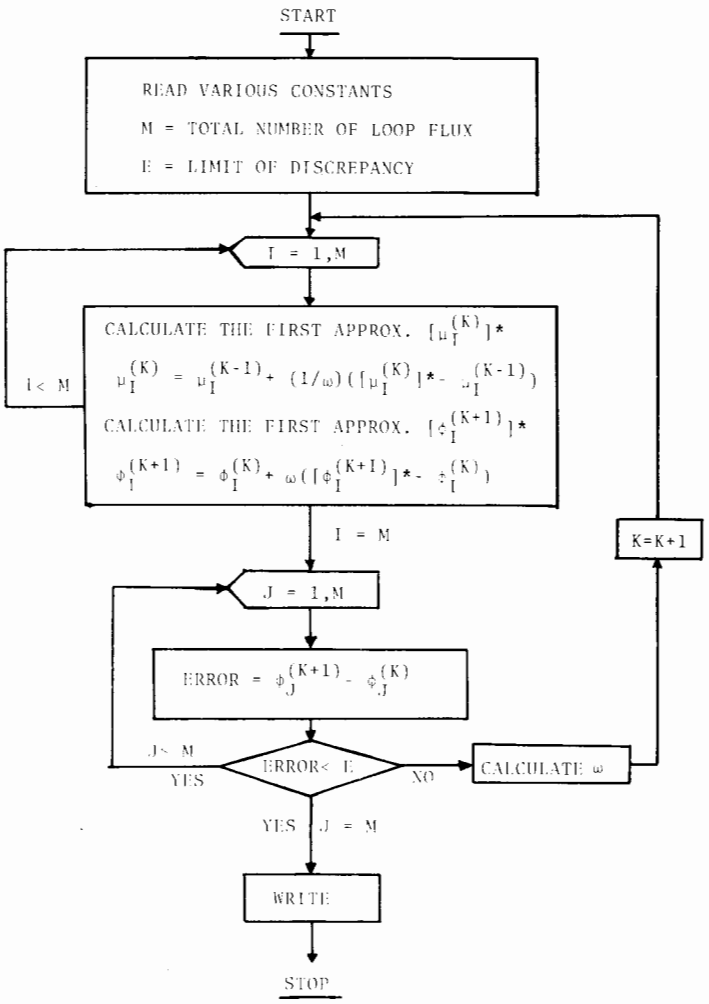

Fig. 4. Flow chart of the iteration method.

Table 2. Various constants used in the calculation

Number of subdivisions in radial direction	9
Number of subdivisions in tangential direction	13
Limit of discrepancy	0.1 percent
Inner radius	0.025 [m]
Outer radius	0.035 [m]
Thickness of iron core	0.01 [m]
Thickness of coil part	0.0025 [m]
Number of turns of coil	250 turns

magnetic field calculations since the magnetic circuit is intrisically defined in three-dimensional space. Moreover, when the magnetic circuit is established, all the boundary conditions that arise in the magnetostatic field problem are automatically taken into account.

The convergence of iterative solutions is fairly improved by the method of this paper, comparing with the method based on experience.

In order to calculate the 104 solutions, it required only 47 seconds for 88 iterations on the computer FACOM 230-45S.

Acknowledgement

The author is grateful to Professor I. Fujita and Professor T. Yamamura for their helpful advice, and to Professor T. Nishiya for the facilities given by him at the computer center of Hosei University. The assistance of Mr. H. Nakagawa, Mr. T. Fujisue and Mr. Y. Nozaki is gratefully acknowledged.

Appendix A. Finite difference equation

For simplicity, it is assumed that fig. 1a in section 2 is written in a rectangular coordinate system.

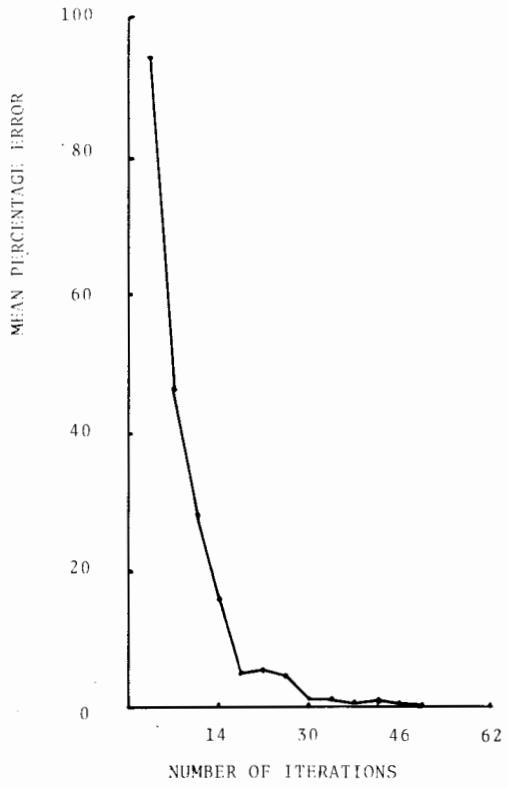

Fig. 5a. Convergence process of the iteration method.

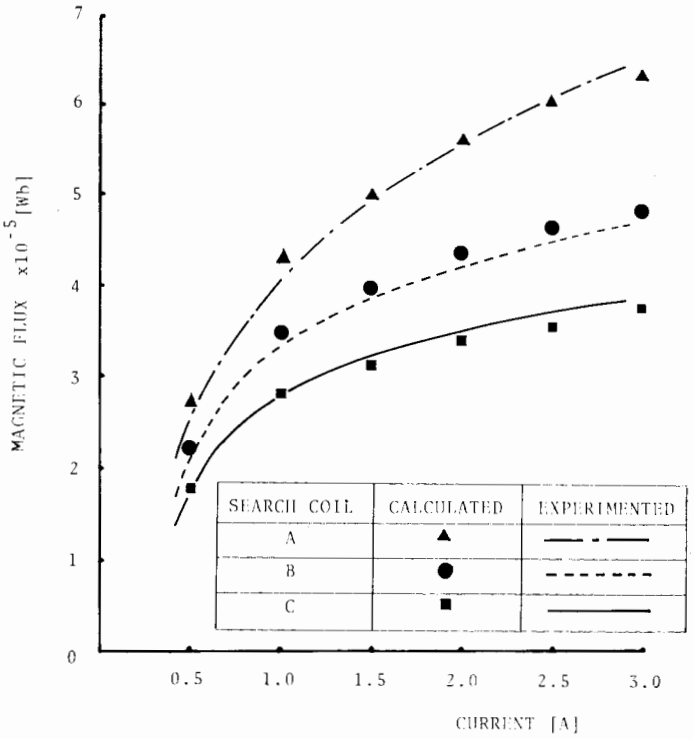

Fig. 5b. Magnetic fluxes in iron core of saturable reactor.

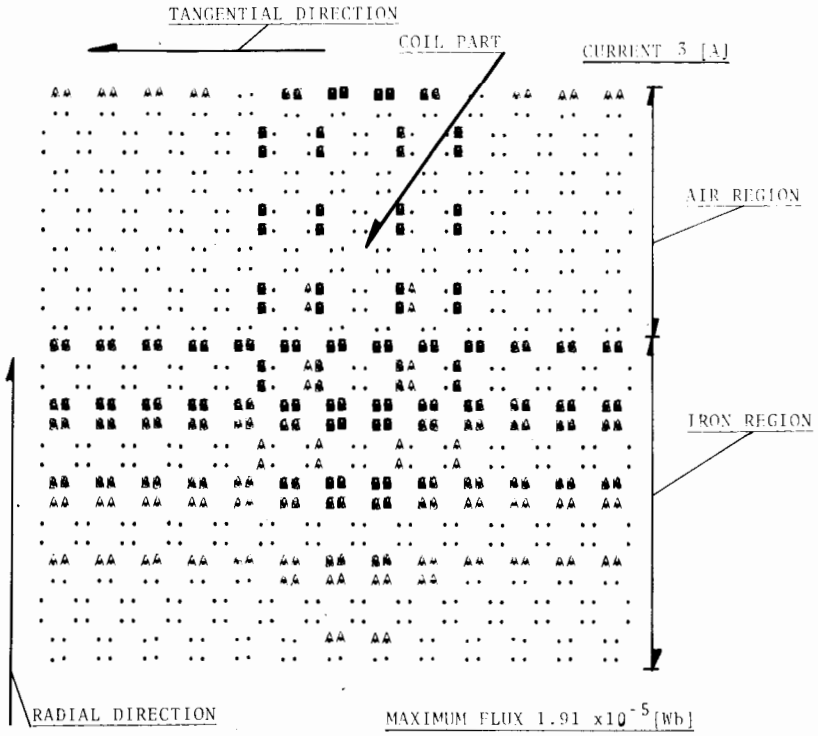

Fig. 5c. Magnetic flux distribution on the magnetic equivalent circuit of saturable reactor.

Then the magnetic field calculation reduces to solving the following partial differential equation [3]:

$$\frac{\partial}{\partial x}\left(\frac{1}{\mu}\frac{\partial A_{i,j}}{\partial x}\right)+\frac{\partial}{\partial y}\left(\frac{1}{\mu}\frac{\partial A_{i,j}}{\partial y}\right)=-J_{i,j}\ , \tag{A.1}$$

where $A_{i,j}$ denotes the vector potential at the mesh point (i, j).

The terms in eq. (A.1) are replaced by the following divided difference approximations [15]:

$$\frac{\partial}{\partial x}\left(\frac{1}{\mu}\frac{\partial A_{i,j}}{\partial x}\right)\cong\frac{1}{h}\left(\frac{A_{i+1,j}-A_{i,j}}{\mu_{i+(1/2),j}h}-\frac{A_{i,j}-A_{i-1,j}}{\mu_{i-(1/2),j}h}\right), \tag{A.2}$$

$$\frac{\partial}{\partial y}\left(\frac{1}{\mu}\frac{\partial A_{i,j}}{\partial y}\right)\cong\frac{1}{g}\left(\frac{A_{i,j+1}-A_{i,j}}{\mu_{i,j+(1/2)}g}-\frac{A_{i,j}-A_{i,j-1}}{\mu_{i,j-(1/2)}g}\right), \tag{A.3}$$

where h and g are respective mesh spacings in the x and y directions; $A_{i+1,j}$, $A_{i-1,j}$, $A_{i,j+1}$, $A_{i,j-1}$ denote the vector potentials at the mesh points $(i+1, j)$, $(i-1, j)$, $(i, j+1)$, $(i, j-1)$; the subscripts $(i+(1/2), j)$, $(i-(1/2), j)$, $(i, j+(1/2))$, $(i, j-(1/2))$ refer to the positions $(x_i+(h/2), y_j)$, $(x_i-(h/2), y_j)$, $(x_i, y_j+(g/2))$, $(x_i, y_j-(g/2))$, respectively.

By substituting eqs. (A.2), (A 3) into eq. (A.1) the finite difference approximation to eq. (A.1) is given by

$$\frac{1}{h^2}\left(\frac{A_{i+1,j}-A_{i,j}}{\mu_{i+(1/2),j}}\right)+\frac{1}{h^2}\left(\frac{A_{i-1,j}-A_{i,j}}{\mu_{i-(1/2),j}}\right)+\frac{1}{g^2}\left(\frac{A_{i,j+1}-A_{i,j}}{\mu_{i,j+(1/2)}}\right)+\frac{1}{g^2}\left(\frac{A_{i,j-1}-A_{i,j}}{\mu_{i,j-(1/2)}}\right)=-J_{i,j}\ , \tag{A.4}$$

or, rearranging,

$$\frac{g}{\mu_{i+(1/2),j}hp}\left(A_{i+1,j}p-A_{i,j}p\right)+\frac{g}{\mu_{i,j-(1/2)}hp}\left(A_{i-1,j}p-A_{i,j}p\right)$$

$$+\frac{h}{\mu_{i,j+(1/2)}gp}\left(A_{i,j+1}p-A_{i,j}p\right)+\frac{h}{\mu_{i,j-(1/2)}gp}\left(A_{i,j-1}p-A_{i,j}p\right)=-ghJ_{i,j}\ . \tag{A.5}$$

Comparison of eq. (A.5) with eq. (5) in section 2 yields the following correspondences:

$$\begin{aligned}R_{i+(1/2)}(\phi_{i,j}-\phi_{i+1,j})&=\frac{g}{\mu_{i+(1/2),j}hp}\left(A_{i,j}p-A_{i+1,j}p\right),\\ R_{i-(1/2)}(\phi_{i,j}-\phi_{i-1,j})&=\frac{g}{\mu_{i-(1/2),j}hp}\left(A_{i,j}p-A_{i-1,j}p\right),\end{aligned} \tag{A.6}$$

$$R_{j+(1/2)}(\phi_{i,j} - \phi_{i,j+1}) = \frac{h}{\mu_{i,j+(1/2)}\, gp}\,(A_{i,j}p - A_{i,j+1}\,p)\,,$$

$$R_{j-(1/2)}(\phi_{i,j} - \phi_{i,j-1}) = \frac{h}{\mu_{i,j-(1/2)}gp}\,(A_{i,j}\,p - A_{i,j-1}\,p)\,, \tag{A.6}$$

$$I_{i,j} = ghJ_{i,j}\,.$$

From eq. (A.6) it is found that eq. (5) is one of the finite difference equations.

Appendix B. Method of determining the relaxation parameter

To determine the relaxation parameter ω, it is assumed that ω is equal to or greater than 1 but smaller then 2 and that the mean percentage error $\varepsilon[\omega(K)]$ for the entire solution (not including the permeabilities) can be expanded thus:

$$1 \leqslant \omega < 2\,, \tag{B.1}$$

$$\varepsilon[\omega^{(K-1)} + \Delta\omega^{(K)}] = \varepsilon[\omega^{(K-1)}] + \Delta\omega^{(K)}\left(\frac{\partial\varepsilon}{\partial\omega}\right)_{\omega=\omega^{(K-1)}} + \tfrac{1}{2}(\Delta\omega^{(K)})^2\left(\frac{\partial^2\varepsilon}{\partial\omega^2}\right)_{\omega=\omega^{(K-1)}} + \ldots\,, \tag{B.2}$$

where $\omega^{(K-1)} + \Delta\omega^{(K)}(= \omega^{(K)})$ is the relaxation parameter used in the Kth iteration, and $\Delta\omega^{(K)}$ denotes the rate of change of the relaxation parameter in the Kth iteration. At the $(K+1)$th iteration the error $\varepsilon[\omega^{(K-1)} + \Delta\omega^{(K+1)}]$ must be set equal to zero by the suitable selection of relaxation parameter. Therefore, neglecting the second-order terms $(\Delta\omega^{(K)})^2$, $(\Delta\omega^{(K+1)})^2$, the rate of change $\Delta\omega^{(K+1)}$ is calculated from

$$\varepsilon[\omega^{(K-1)} + \Delta\omega^{(K+1)}] = \varepsilon[\omega^{(K-1)}] + \Delta\omega^{(K+1)}\left(\frac{\partial\varepsilon}{\partial\omega}\right)_{\omega=\omega^{(K-1)}} = 0\,, \tag{B.3}$$

whence

$$\Delta\omega^{(K+1)} = -\frac{\varepsilon[\omega^{(K-1)}]}{\left(\frac{\partial\varepsilon}{\partial\omega}\right)_{\omega=\omega^{(K-1)}}}\,. \tag{B.4}$$

By combining (B.2) with (B.4) the relaxation parameter in the $(K+1)$th iteration is given by

$$\omega^{(K-1)} + \Delta\omega^{(K+1)} = \omega^{(K-1)} - \frac{\Delta\omega^{(K)}\varepsilon[\omega^{(K-1)}]}{\varepsilon[\omega^{(K-1)} + \Delta\omega^{(K)}] - \varepsilon[\omega^{(K-1)}]}\,. \tag{B.5}$$

The relaxation parameters for the first and second iterations were respectively selected to be 1.5 and 1.6 in the calculations of this paper. Moreover, if eq. (B.5) did not satisfy the condition of eq. (B.1), then the rate of change $\Delta\omega^{(K+1)}$ in the $(K+1)$th iteration was reduced to satisfy this condition.

References

[1] F.C. Trutt, E.A. Erdélyi and R.F. Jackson, The nonlinear potential equation and its numerical solution for highly saturated electrical machines, IEEE Trans. Aerospace AS-1 (1963) 430–440.

[2] E.A. Erdélyi, S.V. Ahamed and R.D. Burtness, Flux distribution in saturated DC machines at no-load, IEEE Trans. Power Apparatus and Systems, PAS-84 (1965) 375–381.

[3] S.V. Ahamed and E.A. Erdélyi, Flux distribution in DC machines on-load and overloads, IEEE Trans. Power Apparatus and Systems, PAS-85 (1966) 960–967.

[4] R.F. Jackson and E.A. Erdélyi, Combination and separation of coordinates and modular programming for DC machine fields, IEEE Trans. Power Apparatus and Systems, PAS-87 (1968) 659–664.

[5] E.A. Erdélyi, M.S. Sarma and S.S. Coleman, Magnetic fields in nonlinear salient pole alternaters, IEEE Trans. Power Apparatus and Systems. PAS-87 (1968) 1848–1856.

[6] E.A. Erdélyi and E.F. Fuchs, Nonlinear magnetic field analysis of DC machines, IEEE Trans. Power Apparatus and Systems, PAS-89 (1970) 1546–1554.

[7] P. Silverster and Madabushi V.K. Chari, Finite element solution of saturable magnetic field problems, IEEE Trans. Power Apparatus and Systems, PAS-89 (1970) 1642–1651.

[8] P. Silverster and A. Konrad, Analysis of transformer leakage phenomena by high-order finite elements, IEEE Power Eng. Society Winter Meeting, T73023-9 (1973) 1843–1851.

[9] A. Foggia, J.C. Sabonnadiere and P. Silverster, Finite element solution of saturated travelling magnetic field problems, IEEE Trans. Power Apparatus and Systems, PAS-94 (1975) 866–871.

[10] O.W. Andersen, Transformer leakage flux program based on the finite element method, IEEE Power Apparatus and Systems, PAS-92 (1973) 682–689.

[11] R. Glowinski and A. Marrocco, Numerical solution of two-dimensional magnetostatic problems by augmented lagrangian methods, Comp. Meths. Appl. Mech. Eng. 12 (1977) 33–46.

[12] R. Glowinski and A. Marrocco, Analyse numérique du champ magnétique d'un alternateur par éléments finis et surrelaxation ponctuelle non linéaire, Comp. Meths. Appl. Mech. Eng. 3 (1974) 55–80.

[13] Y. Saito, Method of magnetic circuits for nonlinear magnetostatic fields in polyphase induction motors at no-load, Comp. Meths. Appl. Mech. Eng. 13 (1978) 105–118.

[14] F.C. Trutt, E.A. Erdélyi and R.E. Hopkins, Representation of the magnetization characteristic of DC machines for computer use, IEEE Trans. Power Apparatus and Systems, PAS-87 (1968) 665–669.

[15] R.S. Varga, Matrix iterative analysis (Prentice-Hall, Englewood Cliffs. NJ, 1962).